

# Characterizing Observed Limit Cycles in the Cassini Main Engine Guidance Control System

Farheen Rizvi<sup>1</sup> and Raquel M. Weitzl<sup>2</sup>

*Jet Propulsion Laboratory, California Institute of Technology, Pasadena, CA, 91109*

The Cassini spacecraft dynamics-related telemetry during long Main Engine (ME) burns has indicated the presence of stable limit cycles between 0.03-0.04 Hz frequencies. These stable limit cycles cause the spacecraft to possess non-zero oscillating rates for extended periods of time. This indicates that the linear ME guidance control system does not model the complete dynamics of the spacecraft. In this study, we propose that the observed limit cycles in the spacecraft dynamics telemetry appear from a stable interaction between the unmodeled nonlinear elements in the ME guidance control system. Many nonlinearities in the control system emerge from translating the linear engine gimbal actuator (EGA) motion into a spacecraft rotation. One such nonlinearity comes from the gear backlash in the EGA system, which is the focus of this paper. The limit cycle characteristics and behavior can be predicted by modeling this gear backlash nonlinear element via a describing function and studying the interaction of this describing function with the overall dynamics of the spacecraft. The linear ME guidance controller and gear backlash nonlinearity are modeled analytically. The frequency, magnitude, and nature of the limit cycle are obtained from the frequency response of the ME guidance controller and nonlinear element. In addition, the ME guidance controller along with the nonlinearity is simulated. The simulation response contains a limit cycle with similar characteristics as predicted analytically: 0.03-0.04 Hz frequency and stable, sustained oscillations. The analytical and simulated limit cycle responses are compared to the flight telemetry for long burns such as the Saturn Orbit Insertion and Main Engine Orbit Trim Maneuvers. The analytical and simulated limit cycle characteristics compare well with the actual observed limit cycles in the flight telemetry. Both have frequencies between 0.03-0.04 Hz and stable oscillations. This work shows that the stable limit cycles occur due to the interaction between the unmodeled nonlinear elements and linear ME guidance controller.

## Nomenclature

$A$	= nonlinear input amplitude
$A_{n1}, A_{n2}, A_{d1}, A_{d2}$	= bi-propellant slosh coefficients
$B_{n1}, B_{n2}, B_{d1}, B_{d2}$	= bi-propellant slosh coefficients
$C_{n1}, C_{n2}, C_{d1}, C_{d2}$	= bi-propellant slosh coefficients
$DSM$	= deep space maneuver
$EGA$	= engine gimbal actuator
$FFT$	= fast fourier transform
$ESA$	= European Space Agency
$G$	= combined ME guidance controller transfer function
$Hz$	= hertz
$h$	= freeplay coefficient
$I_{xx}$	= spacecraft X-axis moment of inertia
$I_{xx-m}$	= spacecraft X-axis moment of inertia parameter (it is a function of the X-axis $I_{xx}$ )
$JPL$	= Jet Propulsion Laboratory

---

<sup>1</sup> Mission Operations Engineer, Guidance & Control Operations, M/S 230-104, 4800 Oak Grove Dr., M.S. 230-104, Pasadena, CA, farheen.rizvi@jpl.nasa.gov

<sup>2</sup> Fault Protection Engineer, End-to-End Information System Engineering, M/S 230-104, 4800 Oak Grove Dr., M.S. 230-104, Pasadena, CA, raquel.m.weitzl@jpl.nasa.gov

$M$	= nonlinear output amplitude
$ME$	= main engine
$mrad$	= milliradian
$N$	= describing function
$NASA$	= National Aeronautics and Space Administration
$OTM$	= orbit trim maneuver
$R$	= commanded and combined dynamics-related telemetry (attitude and rate)
$S/C$	= spacecraft
$SOI$	= Saturn orbit insertion
$T_{TVC}$	= thrust vector control transfer function
$T_{EGA}$	= engine gimballed actuator transfer function
$T_{mag}$	= magnetometer boom dynamics transfer function
$T_{prop}$	= bi-propellant slosh dynamics transfer function
$T_{sc}$	= rigid body spacecraft dynamics transfer function
$TCM$	= trajectory correction maneuver
$TVC$	= thrust vector control
$TWD$	= tail wag dog (force component)
$\Delta E$	= energy change
$\Delta V$	= spacecraft velocity change
$\gamma$	= engine gimballed angle (it is also the input to the nonlinear element)
$\tilde{\theta}$	= estimated and combined dynamics-related telemetry (attitude and rate)
$\theta$	= estimated spacecraft attitude
$\theta_{commanded}$	= commanded spacecraft attitude
$\theta_{control\ system\ estimate}$	= ME guidance controller spacecraft attitude estimate (same as $\theta$ )
$\omega$	= estimated spacecraft body rate about X-axis
$\omega_{commanded}$	= commanded spacecraft X-axis body rate
$\omega_{control\ system\ estimate}$	= ME guidance controller spacecraft X-axis body rate estimate (same as $\omega$ )

## I. Introduction

THE Cassini-Huygens mission is a joint NASA/ESA effort whose primary purpose is to explore Saturn, its rings, and moons. The mission launched from Earth in October 1997 and entered orbit around Saturn in July 2004 by performing two gravity assist-flybys of Venus (1998 and 1999), a flyby of Earth (1999), and one of Jupiter (2000). Cassini also successfully deployed the Huygens probe onto the surface of Titan in 2005.

In order to reach and enter the orbit around Saturn, two long burns were performed with the rocket engine on-board the spacecraft. The Deep Space Maneuver (DSM) lasted 1.46 hours and propelled the spacecraft onto the correct trajectory to reach Saturn. When Cassini reached Saturn, the Saturn Orbit Insertion (SOI) burn was performed for 1.61 hours so the spacecraft could achieve the required orbit around Saturn. SOI, along with its check out burn - TCM-19b - , are unique when compared to all other Cassini burns. These two burns had a target  $\Delta E$  (Energy) instead of a target  $\Delta V$ , which all other burns aim to achieve. In other words, the SOI burn attitude was rotated slowly, or “steered” with a rate of about 0.14 mrad/s. This rate tended to keep the thrust vector opposite the Saturn-relative velocity vector during the burn. Throughout its 1.61 hour SOI burn, the spacecraft attitude was rotated 46.37°. The spacecraft dynamics-related telemetry from the DSM and SOI indicated the presence of stable limit cycles between 0.03-0.04 Hz. Figure 1 shows the time history of the spacecraft X-axis rate, attitude control error, and fast fourier transform (FFT) on the dynamics-related telemetry near the end of the SOI burn.

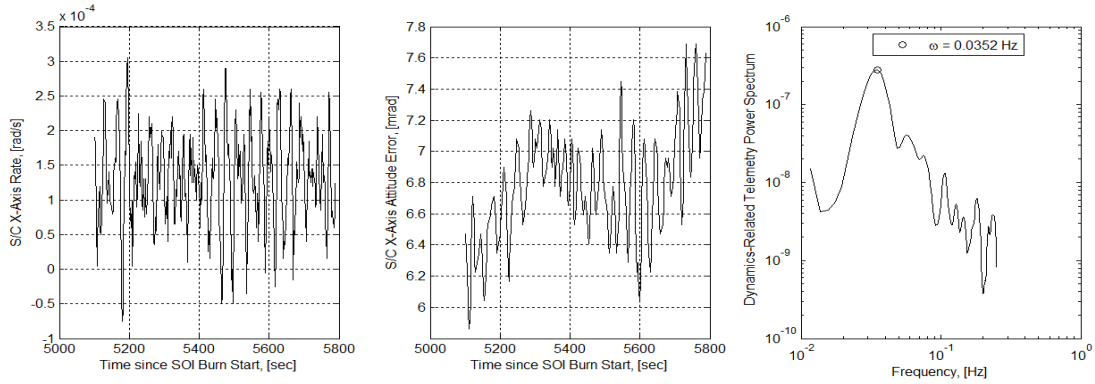


**Figure 1. Spacecraft Dynamics-Related Telemetry Time History and its Fast Fourier Transform Near the End of SOI Burn**

In Fig. 1, the X-axis rate and attitude control error constitute dynamics-related telemetry. The FFT indicates the presence of a stable limit cycle of 0.035 Hz in the telemetry. In the lifetime of the spacecraft, aside from DSM and SOI, the long burns currently performed are the Main Engine (ME) Orbit Trim Maneuvers (OTMs). These are executed so that the spacecraft remains near a trajectory that maximizes interesting science and minimizes propellant usage. Figure 2 depicts the dynamics-related telemetry and its FFT for one of these ME OTMs.

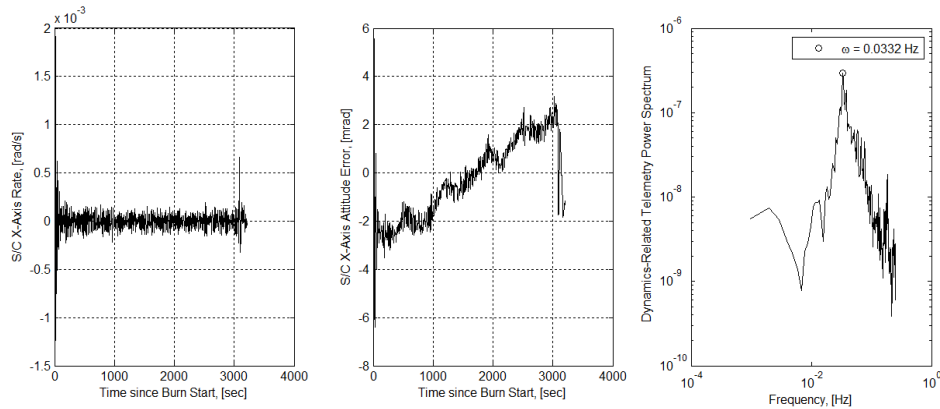


**Figure 2. Spacecraft Dynamics-Related Telemetry Time History and its Fast Fourier Transform for ME OTM 2**

From Fig. 2, a stable limit cycle of 0.033 Hz is observed in the FFT of the telemetry. During and after the ME OTMs, the presence of these limit cycles within the dynamics of the system causes the spacecraft to possess non-zero oscillating rates throughout much of each ME burn. If the dynamics and interaction within the spacecraft are captured accurately, the spacecraft body rates should ideally follow the commanded attitude and stay there throughout the ME burn, enabling the error to decay to zero. Instead, a stable limit cycle is observed indicating that the current ME guidance control system does not model the complete dynamics of the spacecraft system. In order to capture the remaining dynamics, the behavior of these stable limit cycles should be characterized first. We propose that the observed limit cycles in the spacecraft dynamics telemetry appear from a stable interaction between the unmodeled nonlinear elements and the linear ME guidance controller. One such nonlinearity emerges from the gear backlash in the engine gimbal actuator (EGA) system, where the EGA motion is translated into a spacecraft rotation. The limit cycle characteristics and behavior can be predicted by modeling the gear backlash nonlinear element via a describing function and studying the interaction of this describing function with the overall dynamics of the spacecraft.

## II. ME Guidance Controller

The ME guidance controller is used to maintain the required spacecraft attitude during ME burns. The ME system is illustrated in Fig. 3. The spacecraft attitude about each spacecraft axis X, Y, and Z is stabilized by a

different controller. In this paper, we are only concerned with the X-axis control system. X-axis system dynamics contains the spacecraft rigid and flexible body dynamics. The flexible body dynamics model the effects from the magnetometer boom and propellant slosh. The magnetometer boom is attached to the spacecraft body via springs, and sloshing bipropellant is modeled using two pendulums. The higher level diagram for the X-axis control system is shown in Fig. 4. The attitude commander calculates the required spacecraft attitude and rate. This input is sent to the Thrust Vector Controller (TVC), or the attitude controller that controls the spacecraft dynamics. The TVC operates on the spacecraft dynamics error generated from the attitude commander input and feedback from the attitude estimator, and outputs an engine rotation angle. This rotation angle becomes an input to the engine gimbal actuator (EGA) manager which outputs the required engine gimbal angles. The spacecraft rigid body dynamics, magnetometer boom, and bipropellant slosh effects convert this gimbal angle into a spacecraft rotation angle about the X-axis. The attitude estimator (gyro) senses this spacecraft attitude and sends the feedback to the attitude controller. The process continues until error between the commanded and sensed spacecraft dynamics is below the required threshold.

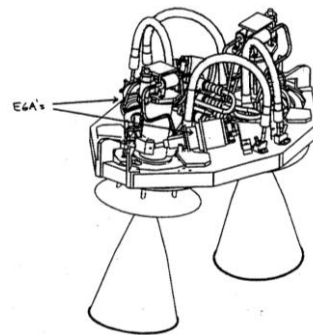


Figure 3. Main Engine Assembly

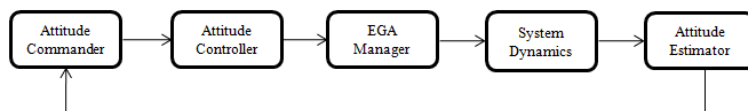


Figure 4. Diagram of X-axis Spacecraft Control System

For the ME guidance controller used in this paper, the control system in Fig. 4 is simplified. The processes within the attitude commander are ignored and the attitude controller has a step input into the system, which symbolizes a constant commanded spacecraft dynamics input. The complexities of the attitude controller are also simplified by removing the simulated filters in the system. The attitude estimator is removed from the system by assuming a perfect sensor for spacecraft dynamics. The performance of this simplified X-axis control system is presented in Fig. 5. The spacecraft rotation angle and rate settle to the commanded rotation angle and rate. It can be concluded that the system exhibits stable behavior.

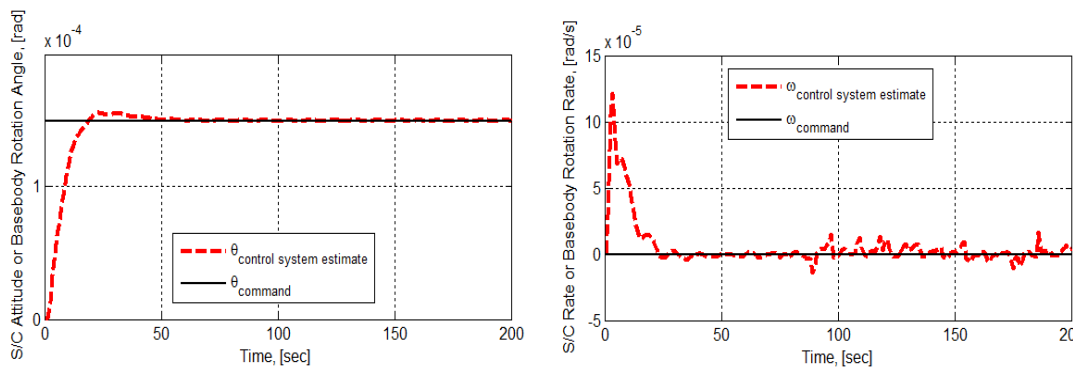


Figure 5. X-axis Control System Performance

### III. Modeling Nonlinearities

The Cassini Main Engine guidance controller is modeled as a linear system, however, in reality the system is nonlinear. Some of these nonlinear elements include backlash in the gears, resistance from propellant flex lines, or other friction mechanisms. For the purposes of this paper, the focus will be on the backlash in the gears.

In linear systems, there are analytical techniques that can be used to model a system completely. However, when dealing with nonlinear systems, there exists dependence between the system response behavior and the magnitude and type of input. Nonlinear systems can produce stable outputs or show instability under certain inputs, thus

making them unstable. Unmodeled nonlinearities in a system can lead to stable limit cycles, which are self-sustained oscillations due to a perturbation. The limit cycle characteristics, frequency, and magnitude of oscillation can be determined experimentally. The limit cycle frequencies in the Cassini dynamical system decreased from 0.050 Hz during the DSM burn to 0.033 Hz after the SOI burn.<sup>2</sup> This indicates that the frequency of the limit cycle oscillations drops with reducing inertia of the spacecraft. Focusing analytical efforts on the SOI burn, it was determined from FFT analysis of the spacecraft X-axis rate that the frequency was 0.033 Hz, and from linear variable differential transformer position telemetry that the magnitude was +0.03-+0.04 mm.<sup>2</sup> One may argue that since the observed limit cycle frequency closely resembles the fundamental frequency of the high-g bi-propellant sloshing motion, which is about 0.05-0.06 Hz, that the stable limit cycle emerges from the sloshing motion. This speculation is rejected because the fuel sloshing motion is modeled by a second-order system whose settling time is  $< 2$  minutes with a natural frequency and damping ratio of 0.05 and 0.12 Hz, respectively,<sup>2</sup> whereas the observed limit cycle oscillations continue for more than an hour. We propose that the sustained limit cycles occur due to a stable interaction between the unmodeled nonlinear elements and linear ME guidance controller. The ME guidance controller and the unmodeled nonlinearities in the system have a stable interaction since the limit cycle amplitude neither dampens, nor grows over time. In order to verify this claim, the nonlinear elements are modeled via a describing function and their interactions with the ME guidance controller are studied. Nonlinear system responses depend upon the amplitude of the input signal. Unlike linear modeling techniques (e.g. transfer functions), the describing function approach captures the dependence of the nonlinear element on the input amplitude.

#### IV. Describing Function

A describing function is a quasilinear representation of a nonlinear element. It is expressed as the complex ratio of the fundamental component of the output to the input signal. This nonlinear analysis approach is used to determine the stability of unforced nonlinear control systems and predict their behavior.

There are a few methods to model nonlinear elements in a system via describing functions; some include hysteresis, on-off, dead-zone, and saturation.<sup>3</sup> In this study, we focus on the nonlinearity that emerges from the gear backlash in the engine gimbal actuators. The best way to capture the input-output characteristics of a gear backlash is through a hysteretic on-off model (see VI. Results and Discussion).

An on-off nonlinearity, also referred to as a two-position nonlinearity, is one whose output is either a positive constant or a negative constant. Figure 6 shows the input-output characteristic curve for both an on-off nonlinearity as well as an on-off with hysteresis.

The main difference between the two is that the nonlinearity containing the hysteretic element incorporates a response lag to the input, which is the best way to characterize the nonlinearity occurring in Cassini TVC algorithm from gear backlash.

Now that a describing function has been chosen to approximately model the backlash nonlinearity, it can be incorporated into the linear ME guidance controller. A unique relationship between the describing function and the linear elements in the ME guidance control system yields stable sustained oscillations. The interaction between the linear ME guidance controller and describing function frequency responses yields the frequency and magnitude of the observed stable limit cycle. The frequency is obtained from the ME guidance controller response, while the describing function yields the amplitude of the observed stable limit cycle. The intersection of the frequency response of the ME guidance controller with the describing function yields the characteristics of the limit cycle. The stability of the oscillations is then determined from the Nyquist condition.<sup>3</sup>

#### V. Model

The ME guidance controller for the X-axis and nonlinear element is shown in Fig. 7.

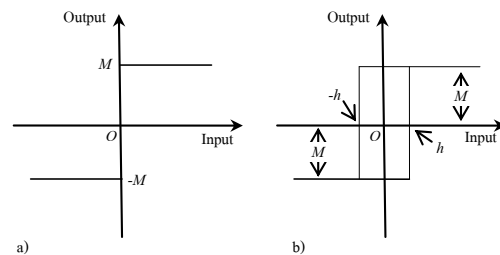


**Figure 6. Input-output characteristic curves for a) on-off nonlinearity; b) on-off nonlinearity with hysteresis**

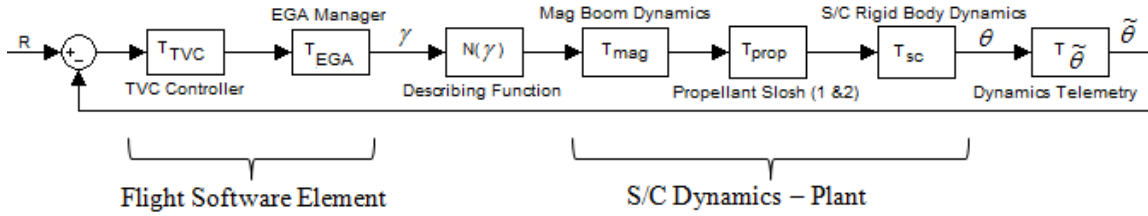


**Figure 7. X-axis Main Engine Guidance Controller and Nonlinear Element**

The error between the commanded dynamics telemetry,  $R$ , and estimated dynamics telemetry,  $\tilde{\theta}$ , is sent to the TVC and then the EGA manager. The output of this error is the required engine gimbal angle,  $\gamma$ . The spacecraft dynamics, including the effects from the magnetometer boom and bipropellant slosh, operate on the  $\gamma$  to yield the estimated spacecraft attitude,  $\theta$ . This  $\theta$  is sent to the transfer function,  $T_{\tilde{\theta}}$ , which combines the estimated spacecraft attitude with the rate and outputs the estimated dynamics telemetry,  $\tilde{\theta}$ . The ratio of the system output,  $\tilde{\theta}$ , to the commanded system input,  $R$ , can be represented by a combined transfer function,

$$R - \tilde{\theta} = \frac{\tilde{\theta}}{T_{TVC} T_{EGA} N T_{mag} T_{prop} T_{sc} T_{\tilde{\theta}}} \rightarrow \frac{\tilde{\theta}}{R} = \frac{T_{TVC} T_{EGA} N T_{mag} T_{prop} T_{sc} T_{\tilde{\theta}}}{1 + T_{TVC} T_{EGA} N T_{mag} T_{prop} T_{sc} T_{\tilde{\theta}}} \quad (1)$$

which comes from equating the elements at the summation junction in Fig. 7. From Eq. (1), the characteristic equation of the system becomes

$$1 + T_{TVC} T_{EGA} N T_{mag} T_{prop} T_{sc} T_{\tilde{\theta}} = 0 \rightarrow \underbrace{T_{TVC} T_{EGA} T_{mag} T_{prop} T_{sc} T_{\tilde{\theta}}}_{G(j\omega)} = \frac{-1}{N(\gamma)} \quad (2)$$

where the linear ME guidance controller elements,  $G$ , are only a function of frequency,  $\omega$ . The nonlinear element,  $N$ , is simplified to only depend upon  $\gamma$ , or the input to the nonlinear element. From the describing function stability analysis<sup>3</sup>, the system output,  $\tilde{\theta}$ , exhibits a limit cycle when Eq. (2) is satisfied. In order to determine when a stable limit cycle occurs and also assess the stability of the system, the frequency responses of  $G$  and  $N$  are examined. The three cases illustrating the interaction between  $G$  and  $N$  responses are shown in Fig. 8.

Figure 8 illustrates the loci of  $G(j\omega)$  and  $-1/N(\gamma)$  evaluated at a range of frequencies,  $\omega$ , and nonlinear input amplitudes,  $\gamma$ . In case a),  $G$  encircles  $N$  and the describing function stability criterion states that the system is unstable<sup>3</sup>. The system output, or amplitude, increases due to any disturbance until breakdown occurs or increases to a value defined by a mechanical stop or safety device. In case b),  $G$  does not enclose  $N$ , indicating a stable system where no limit cycle occurs at steady state.<sup>3</sup> In case c),  $G$  intersects  $N$  and a limit cycle occurs at the corresponding frequency and amplitude determined from the intersection point of  $G(j\omega)$  and  $-1/N(\gamma)$ . The Nyquist and

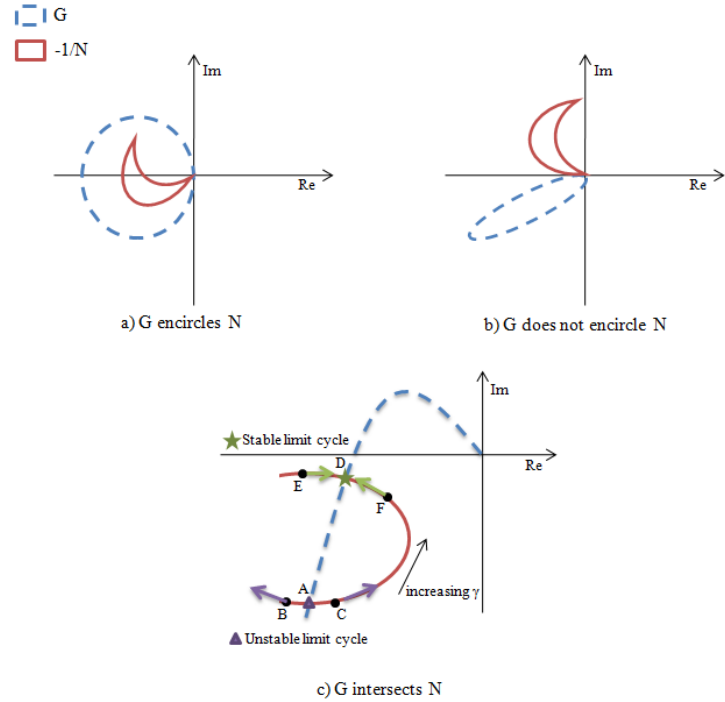


**Figure 8. Linear Elements and Describing Function Interaction for Determining Limit Cycle Stability.** a) Unstable limit cycle, b) No limit cycle, c) Stable or Unstable limit cycle

describing function stability criteria indicate which intersection point produces a stable limit cycle. The Nyquist criterion comments on system stability based upon the encirclements of  $G$  of  $N$ . From this, the describing function stability criterion explains the nature of the limit cycle amplitude.

In this illustration, points  $A$  and  $D$  are the intersection points. First, we consider point  $A$ . If the system is disturbed, the frequency can increase to that at point  $C$ . According to the Nyquist criterion,  $G$  encircles  $N$  at point  $C$  and thus from the describing function stability criterion, the limit cycle amplitude increases towards that of point  $D$ . If the system is disturbed the other way, the frequency can decrease to that at point  $B$ . Here,  $G$  does not encircle  $N$  at point  $B$  and the limit cycle decreases moving further to the left from point  $A$ . Thus, the nature of the system around point  $A$  is divergent and the intersection point  $A$  corresponds to an unstable limit cycle. Next, we examine the stability at point  $D$ . If the system is disturbed and frequency decreases to that at point  $F$ , then  $G$  encircles  $N$  and limit cycle amplitude increases to that at point  $D$ . If the system frequency is increased to that at point  $E$ , then  $G$  does not enclose  $N$  and the limit cycle frequency amplitude decreases to that at point  $D$ . The intersection, point  $D$ , exhibits convergent characteristics and thus corresponds to a stable limit cycle. In practice, only the stable limit cycle is observed.

## VI. Results and Discussion

This section will elaborate on the individual elements of the ME guidance controller in Fig. 7. The model used in this study is evaluated at the launch mass properties for a 50% bipropellant fill. A comparison between the launch, SOI, and model mass properties are shown in Table 1.

Table 1: Mass Properties at Launch and SOI, and Model Mass Properties

	Launch	Pre-SOI	Post-SOI	Model
X-Axis Moment of Inertia, $I_{xx}$ , [kg-m <sup>2</sup> ]	8580	8720	8040	8580
Propellant mass, [kg]	3142	2089	1240	1571
Bipropellant Fill, [%]	100	65	40	50

From Table 1, the model parameters correspond to the properties during the middle of the SOI burn. The data used in this study represents an average of the process during the entire SOI burn. Thus, the current model parameters are used as a decent average for the SOI burn. The components of the TVC block,  $T_{TVC}$ , and the composite transfer function are shown in Fig. 9.

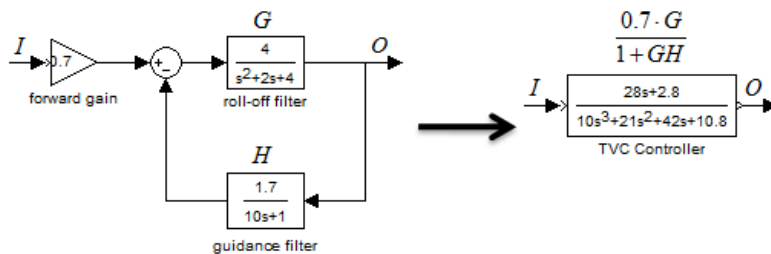


Figure 9. TVC Controller Block

The  $G$  and  $H$  correspond with the roll-off and guidance filters, respectively and  $I$  and  $O$  symbolize the input and output of the TVC. This closed loop system was combined to yield one transfer function for the TVC.

$$0.7I - HO = \frac{O}{G} \rightarrow \frac{O}{I} = \frac{0.7 \cdot G}{1 + GH} = \frac{28s + 2.8}{10s^3 + 21s^2 + 42s + 10.8} \quad (3)$$

The transfer functions for the EGA manager, magnetometer boom, bipropellant slosh, and spacecraft dynamics are given below.

$$\begin{aligned}
T_{EGA} &= \frac{1}{0.036s + 1} \\
T_{mag} &= \frac{0.052s^2 + 0.002s + 1}{0.045s^2 + 0.002s + 1} \\
T_{prop1} &= \frac{A_{n1}s^2 + B_{n1}s + C_{n1}}{A_{d1}s^2 + B_{d1}s + C_{d1}} = \frac{2.74s^2 + 0.033s + 1}{2.55s^2 + 0.033s + 1} \\
T_{prop2} &= \frac{A_{n2}s^2 + B_{n2}s + C_{n2}}{A_{d2}s^2 + B_{d2}s + C_{d2}} = \frac{2.24s^2 + 0.03s + 1}{2.16s^2 + 0.03s + 1} \\
T_{sc} &= \frac{0.0001716s^2 + 0.132}{s^2} \rightarrow \frac{I_{xx-m}}{s^2} = \frac{0.132}{s^2}
\end{aligned} \tag{4}$$

The bipropellant slosh components vary based on the bipropellant fill and mass properties of the spacecraft. The spacecraft rigid body dynamics are a function of the X-axis moment of inertia and thus vary with the changing mass properties. The squared term in the  $T_{sc}$  transfer function in Eqn. (4) is the ‘‘Tail Wags Dog’’, TWD, contribution. TWD represents the tendency of the spacecraft to incur a change in pointing due to the ‘‘tail wagging the dog’’ or the engine thrust affecting the spacecraft. The TWD component from the rigid body dynamics is ignored because its contribution is negligible for this model.

The elements within the dynamics telemetry block,  $T_{\tilde{\theta}}$ , and the composite transfer function are depicted in Fig. 10.

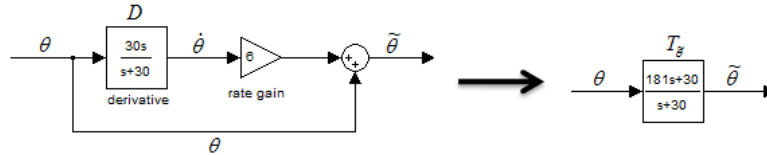


**Figure 10. Dynamics Telemetry Block**

The combined transfer function  $T_{\tilde{\theta}}$  is determined by evaluating the equality at the summation junction in Fig. 10.

$$\theta + 6D\theta = \tilde{\theta} \rightarrow T_{\tilde{\theta}} = \frac{\tilde{\theta}}{\theta} = \frac{181s + 30}{s + 30} \tag{5}$$

The transfer function,  $D$ , is an approximation of the derivative operator,  $s$ , which does not exist in simulink analysis. In this study, the frequencies of interest are  $\sim 0.03$  Hz. When  $D$  is evaluated around these small frequencies, as compared with 30 Hz, the derivative operator is the result.

$$\frac{30s}{s+30} \xrightarrow{j\omega_{small} \approx 0.03Hz} \frac{30s}{30} \rightarrow s \tag{6}$$

In Fig. 7, the  $N(\gamma)$  block accounts for the nonlinearity in the ME guidance controller system. A significant nonlinear component arises from the freeplay, or backlash, in the motor gear system. The motor gear freeplay is due to the loose connection of the teeth between the gears. They are unable to form a tight grip and hence cannot rotate the gear system for very small commanded motions. This means that unless the input signal is above a certain threshold, the gears are not able to produce any output. In order to add nonlinearity, the previously mentioned element called ‘‘on-off nonlinearity with hysteresis’’ is used (see IV. Describing Function). The describing function for this element is

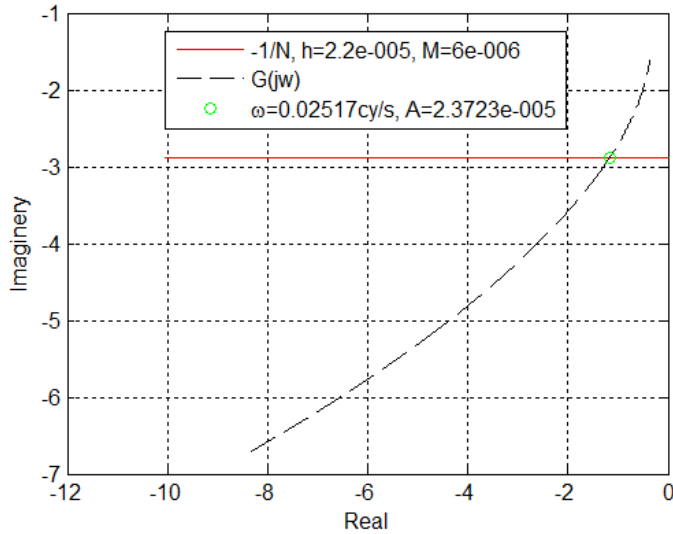
$$N(A = X = \gamma)$$

$$N_{phase} = -\sin^{-1}\left(\frac{h}{X}\right) \quad (7)$$

$$N_{magnitude} = \frac{4M}{\pi X}$$

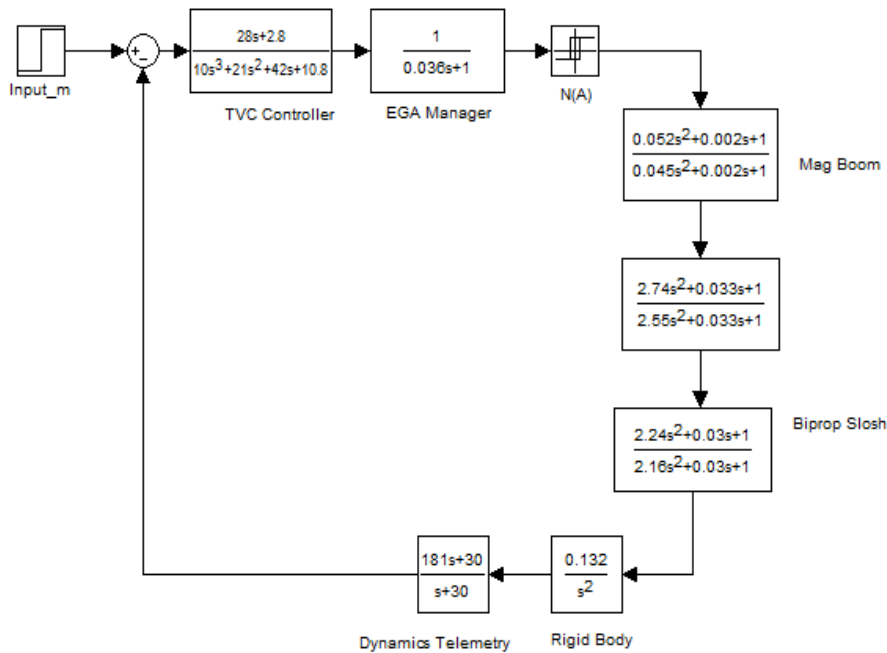
where  $N(A=X=\gamma)$  is a function of the input amplitude. The  $h$ ,  $X$ , and  $M$  are the freeplay coefficient, input signal amplitude and nonlinear element output amplitude, respectively. The  $X$  is also the limit cycle amplitude. The  $h$  is the measure of the threshold above which the system responds to inputs. The model of this element is shown in Fig. 6 b).

As shown before in Fig. 6 b), the output stays at zero and then reaches  $\pm M$  when the threshold increases above  $\pm h$ . In this study, the  $h$  and  $M$  values used are 0.000022 and 0.000006, respectively. These values yield the desired limit cycle and hence capture the system nonlinearity. With the individual transfer functions for all the elements in  $G(j\omega)$  and an analytical expression for  $N(\gamma)$ , Eqn. (2) is evaluated at various frequencies,  $\omega$ , and amplitudes,  $\gamma$ , to yield the result shown in Fig. 11.



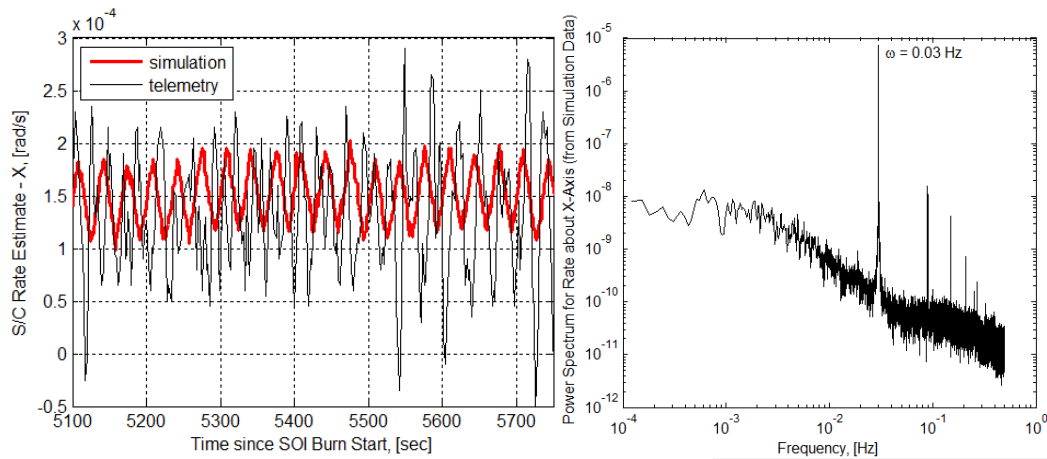
**Figure 11. Analytical Limit Cycle Prediction**

Figure 11 represents the case where  $G$  intersects  $N$ , which indicates a limit cycle in the system response. The Nyquist and describing function criteria are used to determine whether this intersection point corresponds with a stable or unstable limit cycle. In Fig. 11, increasing  $\gamma$  is indicated by a more negative real number. To the right of the intersection point,  $G$  encircles  $N$ . In this case, the limit cycle amplitude increases and moves to the left towards the intersection point. The  $G$  does not enclose  $N$  to the left of the intersection point. Here, the limit cycle amplitude decreases and moves to the right towards the intersection point. In both cases, the intersection is a converging point and thus corresponds to the stable limit cycle behavior (see V. Model). The intersection point corresponds to a frequency,  $\omega=0.025$  Hz and amplitude,  $A=2.4 \times 10^{-5}$  for the limit cycle, thus the describing function theory predicts a stable limit cycle with these characteristics. In order to verify the theory, a simulink model for the X-axis ME guidance controller with the nonlinear element is created, which can be seen in Fig. 12.



**Figure 12. Simulink Model for the Simplified X-axis ME Guidance Controller with Nonlinear Element**

This model is only a representation and simplified version of the actual controller on-board the spacecraft (simplified as per Fig. 4). The simulation output and FFT are presented in Fig. 13.



**Figure 13. Simulated Limit Cycle Prediction and Comparison with SOI Burn Flight Telemetry**

The telemetry data for the X-axis rate from the SOI burn is overlaid on the simulation results. The telemetry exhibits a limit cycle with a dominant frequency of 0.035 Hz and  $0.5 \times 10^{-4}$  amplitude (Fig. 1). In comparison, the simulink model reproduces a limit cycle with 0.030 Hz frequency and  $0.25 \times 10^{-4}$  amplitude. The analytical model predicts a limit cycle of 0.025 Hz frequency and  $0.24 \times 10^{-4}$  amplitude (Fig. 11). The agreement between the telemetry data, simulation output, and analytical prediction verifies that the describing function theory can be used to predict the observed limit cycle. The discrepancies between the telemetry, analytical, and simulation results arise from using a simplified ME guidance controller, inaccurate representation of the actual nonlinearities in the system, and inaccurate model parameters. This model is argued to contain an average measure of the actual model parameters during the SOI burn as shown in Table 1. A sensitivity analysis is performed in order to understand how large of an

impact the model parameters have on the limit cycle characteristics. In this study, the effect of model parameter variations on the limit cycle characteristics are examined. The bipropellant coefficients, moment of inertia parameters, freeplay coefficient, and nonlinear output parameters are varied from  $10^{-1}$  to 10 times the current parameter value used in the model. The effects on the limit cycle frequency and amplitude are shown in Fig. 14, 15, and 16.

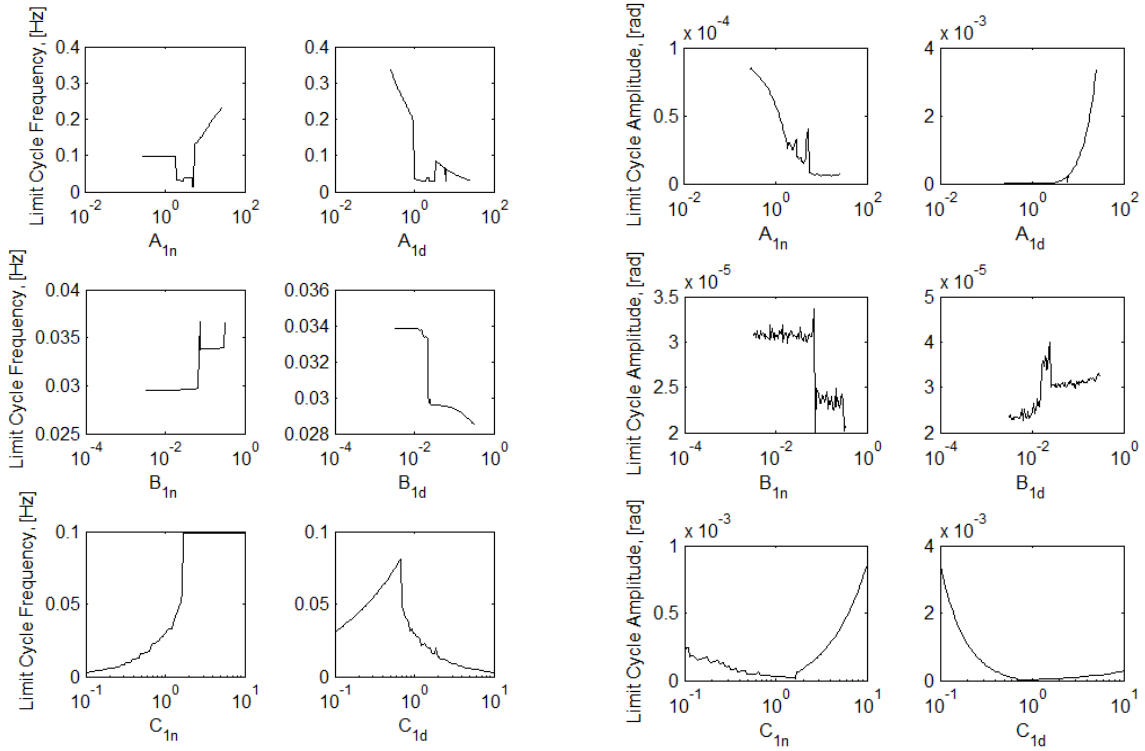
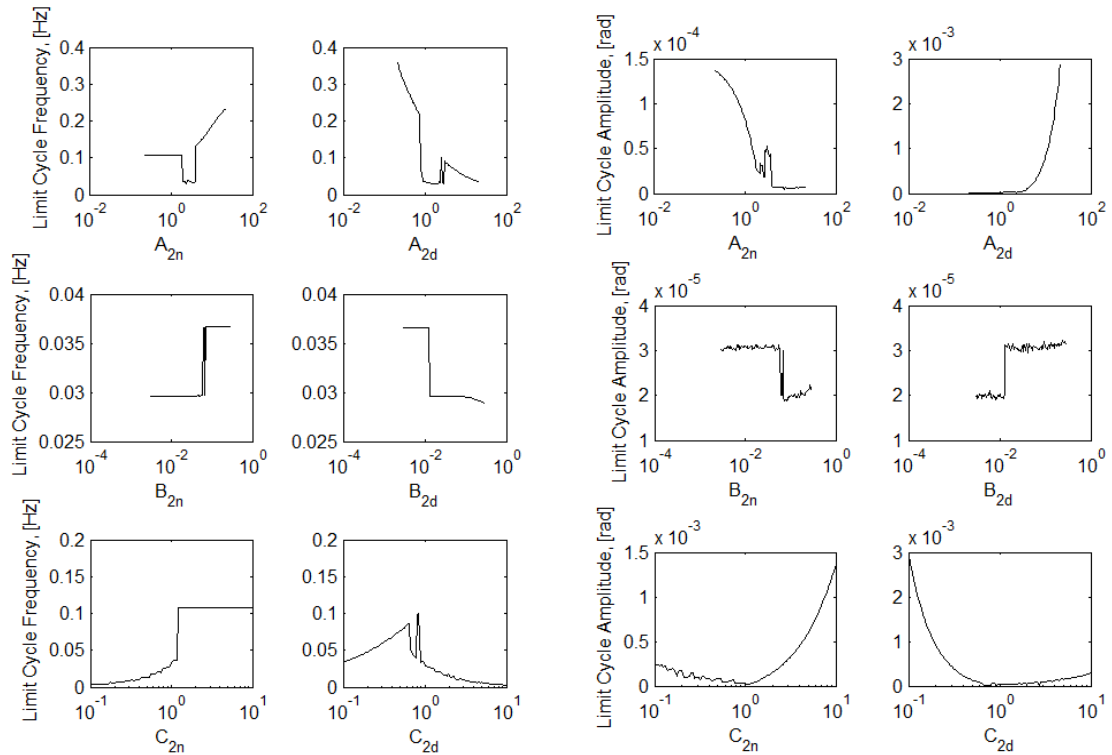
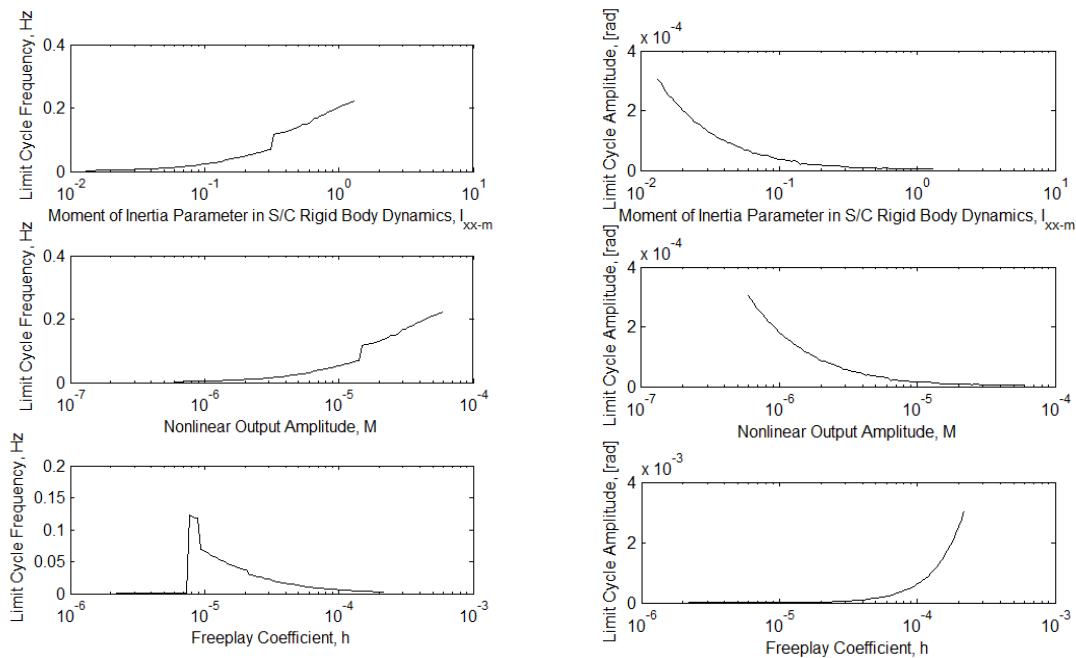


Figure 14. Sensitivity Analysis – Bipropellant Slosh 1 Coefficients



**Figure 15. Sensitivity Analysis – Bipropellant Slosh 2 Coefficients**

In Fig. 14 and 15, the varying coefficients indicate the changing percent of bipropellant slosh in the system. The nature of the sensitivity is similar for both bipropellant 1 and 2 coefficients. The limit cycle frequency and amplitude seem to approach a limiting value as the coefficients increase or decrease. They are not sensitive to deviations around the used model parameters. This means that the model is robust to inaccuracies in capturing the actual bipropellant coefficients, and slight deviations from the actual do not alter the limit cycle characteristics drastically.



**Figure 16. Sensitivity Analysis – Moment of Inertia and Nonlinear Element Parameters**

The moment of inertia parameter is directly proportional to the X-axis moment of inertia. The telemetry data indicates that the limit cycle frequency decreases with decreasing moment of inertia, or in other words with reduced propellant mass.<sup>2</sup> In Fig. 16, the limit cycle frequency decreases as the moment of inertia parameter decreases and thus confirms this finding from the telemetry. The amplitude of the limit cycle increases with reducing moment of inertia and propellant mass. This makes sense because reduced inertia allows the system to move and oscillate more readily. Figure 16 also shows that the limit cycle amplitude increases unboundedly with decreasing moment of inertia and propellant mass. This raises a concern on the type of limit cycle characteristic for the end of mission. The end of mission has the lowest possible propellant mass and thus moment of inertia. In order to better understand the effect of the MOI parameter upon the limit cycle characteristics for greater MOI variations, a larger change in the MOI parameter is examined. The MOI parameter is varied from  $10^{-5}$  to  $10^5$  of the current value used in the model. The results are shown in Fig. 17.

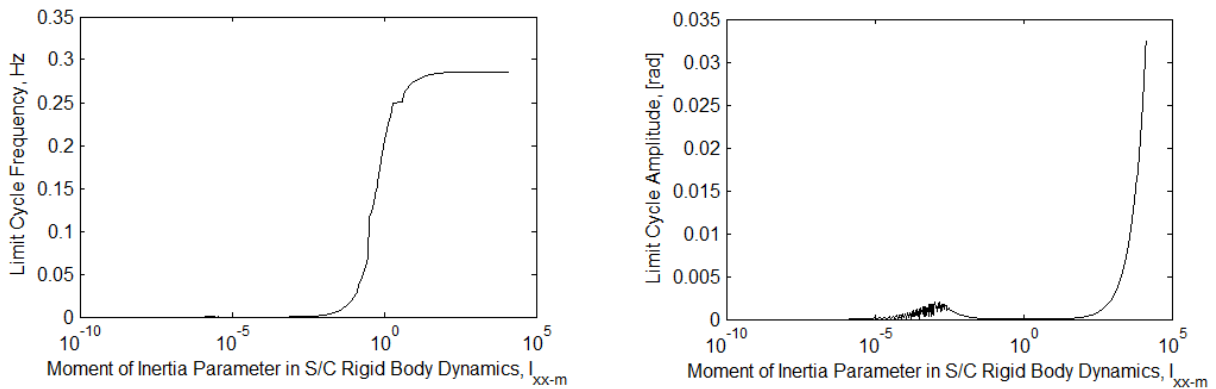


**Figure 17: Sensitivity Analysis – A More Varied Change in the Moment of Inertia Parameter**

In Fig. 17, the limit cycle frequency increases with increasing moment of inertia (MOI) parameter and reaches a limiting value. The amplitude increases, reaching a peak value at an MOI parameter of 0.002 (65 times lower than the one used in the model), decreases, and then increases rapidly with increasing MOI parameter. It can also be concluded that as the spacecraft consumes propellant and moves towards the end of mission, the limit cycle amplitude decreases towards zero. The limit cycle amplitude does not increase unboundedly, which removes any concerns for the end of mission scenario. Also from Fig. 17, a spacecraft with a large moment of inertia results in large amplitude, high frequency limit cycles with the same nonlinearity. Referring back to Fig. 16, the effect on the limit cycle frequency and amplitude with the MOI parameter and nonlinear output amplitude variations exhibit similar characteristics. This means that changing the moment of inertia parameter and nonlinear output amplitude by the same percentage affects the limit cycle frequency and amplitude equally. As the nonlinear output amplitude increases, the period and amplitude of the cycle decrease rapidly. Eventually, this causes the limit cycle to diminish. On the other hand, as the freeplay coefficient increases, the period and amplitude of the cycle increase and grow larger. This means that with increasing the gear backlash intensity (increasing the threshold above which the system responds to inputs), the limit cycles become more prominent and less frequent. The limit cycles have larger amplitudes with less number of cycles per unit time in the system. The input and output characteristics of the nonlinearity in this model are shown in Fig. 18.

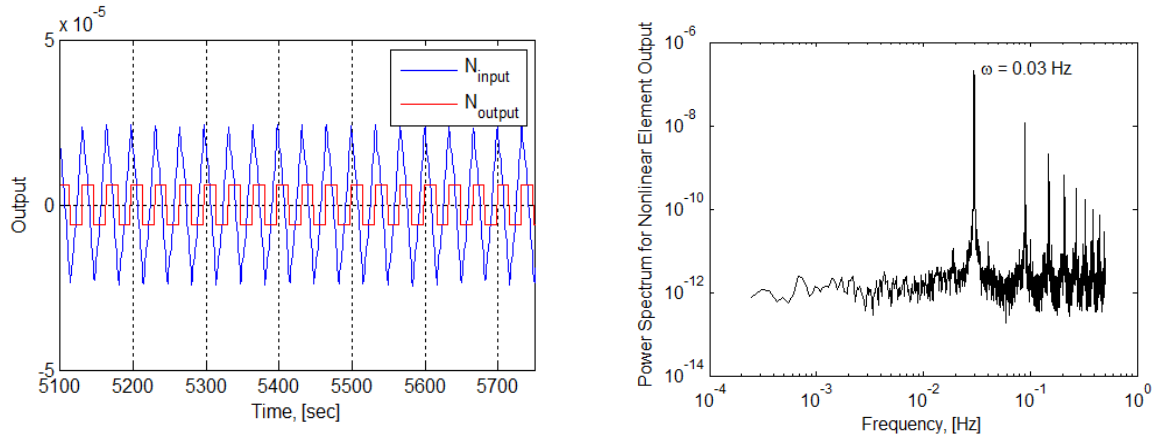


**Figure 18: Nonlinear Input and Output Characteristics**

From Fig. 18, the nonlinear element responds to the sinusoidal input and outputs a square wave. The amplitude of the square wave is the  $M$  value of  $0.6 \times 10^{-5}$ , as expected. The FFT on the nonlinear output has the same dominant oscillating frequency as the system output seen in Fig. 13. This is because the nonlinear element drives the limit cycle in the system and without the nonlinearity the linear system does not exhibit any limit cycle as shown in Fig. 5.

Even though the sustained limit cycle behavior does not pose any significant concerns during spacecraft operations, from a controller design viewpoint, it is important to understand the reason behind the limit cycle existence. This analysis explains the existence of a sustained limit cycle observed in the spacecraft X-axis body rate telemetry from the describing function approach. The stable interaction between the modeled nonlinearity and linear ME guidance controller reproduces the observed limit cycle. With this analysis, a phenomenon is presented that explains the presence of these limit cycles after long burns. In the current life of the mission, long burns occur during the ME OTMs. The dynamics-related telemetry data from the longest ME OTM burns (OTMs 10, 33, and 144) is presented in Fig. 19.

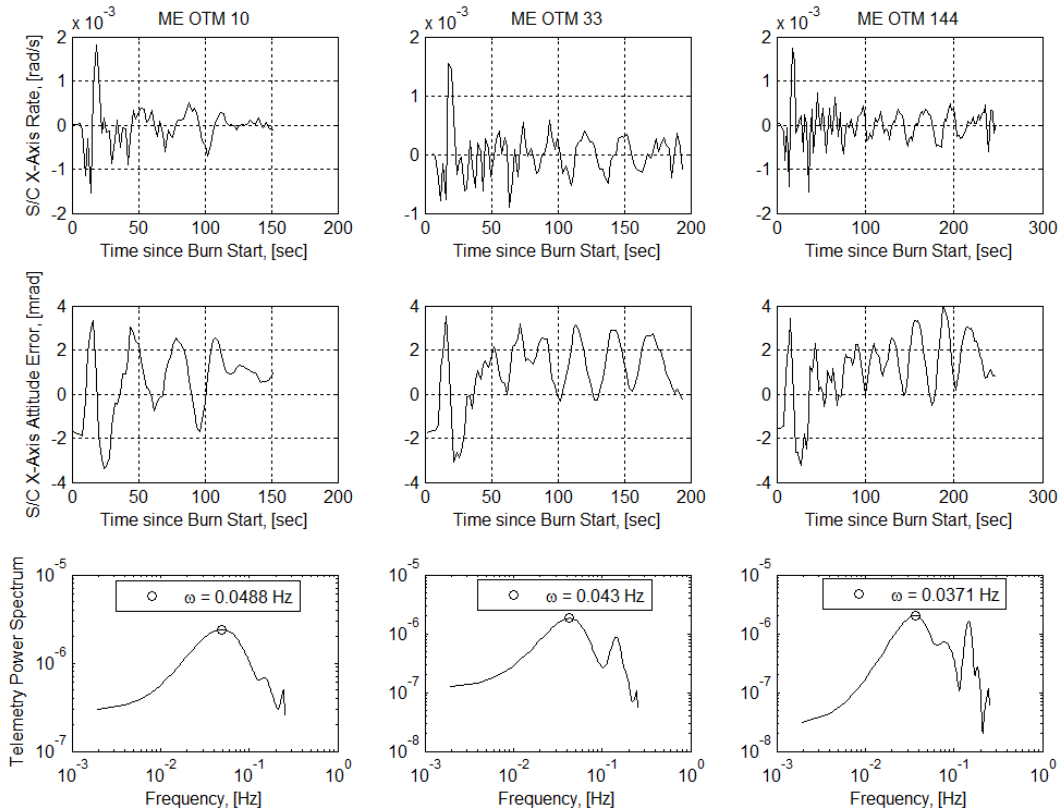


**Figure 19: Main Engine Orbit Trim Maneuver Telemetry Data**

Orbit Trim Maneuvers 10, 33, and 144 are considered long burns with durations 150 s, 200 s, and 250 s, respectively. From Fig. 19, the limit cycle oscillating frequencies are between 0.03-0.05Hz, which agree with that from the other long burns like SOI (Fig. 1) and ME OTM 2 (Fig. 2), and are also consistent with the limit cycle frequencies obtained from the analytical (Fig. 11) and simulated (Fig. 13) models. Discrepancies occur due to different model parameters at the time of OTMs as opposed to the ones used in this analysis. However, the nature of the limit cycle and reason for its presence are explained from this analysis.

## VII. Conclusion

In this study, the presence of the stable limit cycles in the ME guidance control system response are explained. The linear ME guidance controller does not predict limit cycles, which are observed in all dynamics related telemetry after long burns. The limit cycles emerge due to a stable interaction between the linear controller and unmodeled nonlinearities in the system. One such nonlinearity emerges from the motor gear backlash. This is represented via a describing function, and its interaction is studied in conjunction with the ME guidance controller. The analytical theory and simulation results agree with the observed limit cycle characteristics from the SOI burn and ME OTM telemetry. The stable limit cycle frequency settles between 0.03-0.04 Hz for the X-axis rate in these burns.

Discrepancies in this work and actual results occurred because the exact model during the SOI burn and ME OTMs was not available. An assumed average for the model parameters was used. However, it was found that variations from the average model parameters did not affect the limit cycle characteristics drastically. Discrepancies also occurred because the complexities within the ME guidance controller such as filters and spacecraft attitude estimator were ignored and a simplified ME guidance controller model was used instead. For future work, a more accurate model for the ME guidance controller can be used to yield better results. In this study, only the nonlinear effect from the motor gear backlash was considered. For future work, all the nonlinearities in the system can be modeled and their interactions can be studied with the linear ME guidance controller for more accurate results.

For the spacecraft, the limit cycle presence in the Cassini system has not hindered the performance to any degree of concern, however, it is important to understand these stable limit cycles from the controller design viewpoint. In this analysis, the describing function approach is used to explain the presence of these limit cycles during all long burns. In order to avoid the presence of limit cycles in the system, a nonlinear controller could be designed that captures the various nonlinearities in the system and counteract these effects on the system output.

### **Acknowledgments**

This research was carried out at the Jet Propulsion Laboratory, California Institute of Technology, under a contract with the National Aeronautics and Space Administration. The authors would like to acknowledge the efforts of Allan Y. Lee and Glenn A. Macala, who laid the foundations of this present work. Other acknowledgements include Thomas A. Burk for his historical background on AACCS history from SOI.

### **References**

- <sup>1</sup>Enright, P., "Thrust Vector Control Algorithm Design for the Cassini Spacecraft," *AIAA/AHS/ASEE Aerospace Design Conference*, Irvine, California, February 16-19, 1993. AIAA paper 1993-1043.
- <sup>2</sup>Lee, A. Y., and Hanover, G., "Cassini Spacecraft Attitude Control System Flight Performance," *Proceedings of the AIAA Guidance, Navigation, and Control Conference, and Exhibit*, San Francisco, California, August 15-18, 2005.
- <sup>3</sup>Ogata, K., *Modern Control Engineering*, Prentice Hall Inc, New Jersey, 1970, Chap.11.